The Stannides $LaRhSn_2$ and $CeRhSn_2$

Dirk Niepmann, Rainer Pöttgen,* Bernd Künnen, and Gunter Kotzyba

Anorganisch-Chemisches Institut, Universität Münster, Wilhelm-Klemm-Strasse 8, D-48149 Münster, Germany

Carsten Rosenhahn and Bernd D. Mosel*

Institut für Physikalische Chemie, Universität Münster, Schlossplatz 4/7, D-48149 Münster, Germany

Received January 22, 1999. Revised Manuscript Received March 8, 1999

The new stannides $LaRhSn_2$ and $CeRhSn_2$ have been prepared in quantitative yield by reacting the elements in an arc-melting furnace and subsequent annealing at 970 K. Their structures were determined from X-ray single crystal and powder data: *Cmcm*, $a = 460.3(2)$ pm, $b = 1702.9(7)$ pm, $c = 961.3(3)$ pm, $wR2 = 0.0513$, 1317 F^2 values, 30 variables for a $CeRhSn_2$ single crystal and $a = 463.9(1)$ pm, $b = 1710.0(3)$ pm, $c = 963.7(2)$ pm, $R_F = 3.25$, 247 F values, 25 parameters for a $LaRhSn_2$ powder sample. Striking structural motifs of $LaRhSn_2$ and $CeRhSn_2$ are distorted $RhSn_5$ square pyramids which are condensed via common tin atoms and via Sn−Sn bonds forming a three-dimensional infinite $[RhSn_2]$ polyanion. The latter is characterized by strong Rh−Sn (262−277 pm) as well as Sn−Sn (281 pm) interactions. The cerium atoms fill distorted pentagonal and hexagonal channels within the polyanion. Both crystallographically independent cerium atoms have high coordination numbers: 4Ce + 6Rh + 9Sn for Ce1 and 6Ce + 4Rh + 10Sn for Ce2. Magnetic susceptibility measurements indicate Pauli paramagnetism for $LaRhSn_2$ and Curie−Weiss behavior (2.56(2) μ_B/Ce) for $CeRhSn_2$. At 4.0(2) K, $CeRhSn_2$ orders ferro- or ferrimagnetically. The experimental saturation magnetization is 0.75(2) μ_B/Ce at 5.5 T and 2 K. $LaRhSn_2$ and $CeRhSn_2$ are metallic conductors with room-temperature values of 85 ± 20 $\mu\Omega$ cm ($LaRhSn_2$) and 100 ± 20 $\mu\Omega$ cm ($CeRhSn_2$) for the resistivity. The resistance of $CeRhSn_2$ shows a broad minimum near 30 K, possibly suggesting some Kondo-type interactions. Despite the three crystallographically different tin sites the ^{119}Sn Mössbauer spectroscopic measurements show only one signal at $\delta = 1.93(1)$ mm/s ($LaRhSn_2$) and $\delta = 2.01(2)$ mm/s ($CeRhSn_2$), subjected to quadrupole splitting of $\Delta E_Q = 1.29(1)$ mm/s ($LaRhSn_2$) and $\Delta E_Q = 1.38(2)$ mm/s ($CeRhSn_2$).

Introduction

Intermetallic cerium compounds have attracted widespread attention in recent years because of their puzzling physical properties such as long-range magnetic ordering, Kondo effects, magnetic ordering with anomalously high ordering temperatures, the coexistence of heavy-fermion behavior and superconductivity or valence fluctuation behavior.[1−3] The reason for these unusual properties is mostly the hybridization of the 4f electrons with the conduction electrons. Most compounds with cerium in the stable trivalent oxidation state ([Xe]$4f^1$ configuration) show antiferromagnetic ordering at low temperature, while only few compounds order ferromagnetically. The recent investigations have mainly focused on compounds with the simple compositions CeTX and CeT_2X_2 (T = transition metal; X = element of the p block).[1−3] Most of these compounds have highly symmetric structures. This facilitates the understanding of the physical properties and the theoretical treatment.

In the course of our investigations on structure−property relationships of intermetallic cerium compounds[4−12] we have now synthesized the stannides $LaRhSn_2$ and $CeRhSn_2$ which crystallize with a new structure type. The synthesis, structure refinements, and physical properties are reported herein. A brief

(1) Fujita, T.; Suzuki, T.; Nishigori, S.; Takabatake, T.; Fujii, H.; Sakurai, J. *J. Magn. Magn. Mater.* **1992**, *108*, 35.
(2) Szytuła, A.; Leciejewicz, J. *Handbook of Crystal Structures and Magnetic Properties of Rare Earth Intermetallics*; CRC Press: Boca Raton, 1994.
(3) Nieuwenhuys, G. J. Heavy Fermions and Related Compounds. In *Handbook of Magnetic Materials*; Buschow, K. H. J., Ed.; Elsevier: Amsterdam, 1995; Vol. 9, Chapter 1
(4) Gordon, R. A.; DiSalvo, F. J.; Pöttgen, R. *J. Alloys Compd.* **1995**, *228*, 16.
(5) Pöttgen, R.; Borrmann, H.; Kremer, R. K. *J. Magn. Magn. Mater.* **1996**, *152*, 196.
(6) Pöttgen, R.; Borrmann, H.; Felser, C.; Jepsen, O.; Henn, R.; Kremer, R. K.; Simon, A. *J. Alloys Compd.* **1996**, *235*, 170.
(7) Gordon, R. A.; DiSalvo, F. J.; Pöttgen, R.; Brese, N. E. *J. Chem. Soc., Faraday Trans.* **1996**, *92*, 2167.
(8) Gordon, R. A.; DiSalvo, F. J.; Pöttgen, R. *J. Alloys Compd.* **1996**, *236*, 86.
(9) Gordon, R. A.; Warren, C. J.; Alexander, M. G.; DiSalvo, F. J.; Pöttgen, R. *J. Alloys Compd.* **1997**, *248*, 24.
(10) Jones, C. D. W.; Gordon, R. A.; DiSalvo, F. J.; Pöttgen, R.; Kremer, R. K. *J. Alloys Compd.* **1997**, *260*, 50.
(11) Pöttgen, R.; Hoffmann, R.-D.; Sampathkumaran, E. V.; Das, I.; Mosel, B. D.; Müllmann, R. *J. Solid State Chem.* **1997**, *134*, 326.
(12) Prots', Yu. M.; Pöttgen, R.; Niepmann, D.; Wolff, M. W.; Jeitschko, W. *J. Solid State Chem.* **1999**, *142*, 400.
(13) Niepmann, D.; Pöttgen, R. *Z. Kristallogr.* **1999**, Suppl. 16, 51.

10.1021/cm991006u CCC: $18.00
Published on Web 05/11/1999

Table 1. Crystal Data and Structure Refinement for $CeRhSn_2$

empirical formula	$CeRhSn_2$
formula weight	480.41 g/mol
crystal system	orthorhombic
space group	*Cmcm* (no. 63)
lattice constants	$a = 460.3(2)$ pm
(Guinier data)	$b = 1702.9(7)$ pm
	$c = 961.3(3)$ pm
	$V = 0.7535(2)$ nm^3
formula units per cell	$Z = 8$
calculated density	8.47 g/cm^3
crystal size	$10 \times 20 \times 40$ μm^3
transmission ratio (max:min)	1.26
absorption coefficient	29.0 mm^{-1}
$F(000)$	1624
θ range for data collection	2 to 40°
range in hkl	$\pm 8, \pm 30, \overline{17} < l < 1$
total no. reflections	4856
independent reflections	1317
reflections with $I > 2\sigma(I)$	878
data/restraints/parameters	1317/0/30
goodness-of-fit on F^2	1.008
final R indices [$I > 2\sigma(I)$]	$R1 = 0.0227$
	$wR2 = 0.0415$
indices (all data)	$R1 = 0.0588$
	$wR2 = 0.0513$
extinction coefficient	0.00021(2)
largest diff. peak and hole	3675 and −2565 e/nm^3

account of some of this work was given recently at a conference.[13]

Experimental Procedures

Synthesis. Starting materials for the synthesis of $LaRhSn_2$ and $CeRhSn_2$ were ingots of cerium (Johnson Matthey) and lanthanum (Kelpin), rhodium powder (200 mesh, Degussa), and tin bars (Heraeus), all with stated purities better than 99.9%. In a first step the rare earth ingots were cut into small pieces and melted to buttons in an arc-melting furnace[14] under an argon atmosphere. This premelting procedure minimizes a shattering of these elements during the strongly exothermic reactions with rhodium and tin. The argon was purified before over titanium sponge and molecular sieves. In the second step the lanthanoid buttons were arc-melted together with cold-pressed pellets of rhodium powder and with pieces of the tin bar in the ideal atomic ratio 1:1:2. The buttons were turned over and remelted at least four times to achieve homogeneity. The total weight losses during the arc-melting procedures were all smaller than 0.5 weight %. Subsequently, parts of the melted ingots were sealed in evacuated silica ampules and annealed at 970 K for 2 weeks. Both compounds are dark gray in polycrystalline form while single crystals exhibit metallic luster. These stannides are stable in moist air over long periods of time. The samples were routinely characterized by EDX analyses of polished ingots. A Leica 420 I scanning electron microscope was used with LaB_6, CeO_2, rhodium, and tin as standards. The compositions of our samples were very close to the ideal values. No impurity elements heavier than sodium ($Z = 11$) were observed. The analyses of the polished samples in the backscattering mode showed only the compositions $LaRhSn_2$ and $CeRhSn_2$ and no secondary impurity phase.

Structural Characterization. The samples were routinely characterized through their Guinier powder patterns using Cu $K_{\alpha 1}$ radiation and α quartz ($a = 491.30$ pm, $c = 540.46$ pm) as an internal standard. The patterns could completely be indexed on the basis of orthorhombic *C*-centerd cells with the lattice parameters listed in Tables 1 and 2. To ensure correct indexing, the observed patterns were compared with calculated ones,[15] taking the positions of the refined structures.

Table 2. Crystal Data and Structure Refinement for $LaRhSn_2$

empirical formula	$LaRhSn_2$
formula weight	479.20 g/mol
crystal system	orthorhombic
space group	*Cmcm* (no.63)
lattice constants	$a = 463.9(1)$ pm
(Guinier data)	$b = 1710.0(3)$ pm
	$c = 963.7(2)$ pm
	$V = 0.7645(2)$ nm^3
formula weight per cell	$Z = 8$
calculated density	8.33 g/cm^3
absorption coefficient	219.6 mm^{-1}
F(000)	1616
range in 2θ	5 to 99.98°
scan mode, step width	$\omega/2\theta$, 0.02°
scan speed	98.5 s per step
no. data points	4750
total no. Bragg reflections	247
total measuring time	130 h
profile function	pseudo-Voigt
no. variables	25
R_F, R_{wp}	3.25, 6.06
$R_{Bragg(I)}$, goodness-of-fit (χ^2)	5.20, 4.05

Single crystals of $CeRhSn_2$ were isolated from the annealed sample by mechanical fragmentation. They were investigated on a Buerger precession camera to establish both symmetry and suitability for intensity data collection. The photographs showed a *C*-centered orthorhombic cell and the extinction conditions were compatible with space group *Cmcm*. Intensity data were recorded at room temperature with the use of a four-circle diffractometer (CAD4) with graphite-monochromatized Mo K_α radiation and a scintillation counter with pulse−height discrimination. The scans were taken in the $\omega/2\theta$ mode and an empirical absorption correction was applied on the basis of Ψ-scan data.

Starting atomic parameters were deduced from an automatic interpretation of direct methods with SHELXS,[16] and the structure was sucessfully refined with anisotropic displacement parameters using SHELXL-97[17] (full-matrix least-squares on F^2).

The refinement readily converged to the residuals listed in Table 1, and a subsequent difference Fourier synthesis revealed no significant residual peaks. All relevant crystallographic details are listed in Table 1. Atomic coordinates and interatomic distances are given in Tables 3 and 4. As a check for the correct composition, the occupancy parameters were varied in a separate series of least-squares cycles along with the displacement parameters. The occupancies varied between 99.7(2)% for Ce1 and 100.1(3)% for Sn3. Thus, all sites were fully occupied within two standard deviations, and in the final cycles the ideal composition was assumed. Listings of the anisotropic displacement parameters and the structure factors are available.[18]

The structure of $LaRhSn_2$ was refined from X-ray powder data since no suitable single crystals could be found. The intensity data (Figure 1) were recorded from a flat rotating sample consisting of fine-grained $LaRhSn_2$ powder (prepared under dried *n*-hexane in a boron−carbide mortar) which was glued to a thin acetate foil with a silicon grease. A Stoe STADI P powder diffractometer with germanium monochromatized Cu $K_{\alpha 1}$ radiation was used. The data set was recorded in eight subsequent ranges with a counting time of about 16 h per range. These ranges showed no intensity drop over the data collection period, and they were merged for the later refinement. The atomic positions of $CeRhSn_2$ were taken as starting values and the $LaRhSn_2$ structure was subsequently refined

(14) Pöttgen, R.; Gulden, Th.; Simon, A. *GIT Labor-Fachzeitschrift* **1999**, *43*, 133.

(15) Yvon, K.; Jeitschko, W.; Parthé, E. *J. Appl. Crystallogr.* **1977**, *10*, 73.

(16) Sheldrick, G. M. *SHELXS, Program for the Solution of Crystal Structures*; University of Göttingen: Germany, 1997.

(17) Sheldrick, G. M. *SHELXL-97, Program for Crystal Structure Refinement*; University of Göttingen: Germany, 1997.

(18) Details may be obtained from: Fachinformationszentrum Karlsruhe, D-76344 Eggenstein-Leopoldshafen (Germany), by quoting the Registry No's CSD-410732 ($LaRhSn_2$) and CSD-410733 ($CeRhSn_2$).

Table 3. Atomic Coordinates and Isotropic Displacement Parameters for $LaRhSn_2$ and $CeRhSn_2$

$LaRhSn_2$ (X-ray Powder Data)

atom	Wyckoff site	*x*	*y*	*z*	B_{iso}[a]
La1	4c	0	0.2976(2)	1/4	1.06(6)
La2	4b	0	1/2	0	1.06(6)
Rh	8f	0	0.1485(2)	0.5069(4)	1.48(8)
Sn1	8f	0	0.3039(2)	0.5889(3)	1.74(5)
Sn2	4c	0	0.0921(3)	1/4	1.74(5)
Sn3	4c	0	0.9277(3)	1/4	1.74(5)

$CeRhSn_2$ (Single-Crystal Data)

atom	Wyckoff site	*x*	*y*	*z*	U_{eq}[b]
Ce1	4c	0	0.29565(3)	1/4	71(1)
Ce2	4b	0	1/2	0	103(1)
Rh	8f	0	0.14662(3)	0.50464(5)	72(1)
Sn1	8f	0	0.30208(2)	0.58974(5)	72(1)
Sn2	4c	0	0.09125(4)	1/4	103(1)
Sn3	4c	0	0.92629(3)	1/4	83(1)

[a] B_{iso} is given in units of Å^2. The isotropic displacement parameters for the positions with equal elements have been constrained. [b] U_{eq} (pm^2) is defined as one-third of the trace of the orthogonalized U_{ij} tensor.

using the Rietveld least-squares program FULLPROF.[19] A total of 25 parameters were refined: 7 positional parameters, 3 isotropic displacement parameters, 4 profile parameters, 4 asymmetry parameters, 2 parameters for preferred orientation, 3 parameters for the lattice constants, 1 overall scale factor, and 1 zeropoint parameter. Details of the data collection and the refinement are listed in Table 2; atomic parameters and interatomic distances are given in Tables 3 and 4. Additional material on the refinement is deposited.[18]

Physical Property Measurements. The magnetic susceptibilities of polycrystalline pieces of $LaRhSn_2$ and $CeRhSn_2$ were determined with a SQUID magnetometer (Quantum Design, Inc.) between 2 and 300 K with magnetic flux densities up to 5.5 T. The specific resistivities were measured on irregularly shaped polycrystalline blocks with a conventional four-point technique. Cooling and heating curves measured between 4.2 and 300 K were identical within the error limits, also for different samples. ^{119}Sn Mössbauer spectroscopic experiments were performed at absorber temperatures between 300 and 4.2 K on the same polycrystalline samples as used for the susceptibility and resistivity measurements. The $Ca^{119m}SnO_3$ source was held at room temperature and a palladium foil of 0.05 mm thickness was used to reduce the tin K X-rays concurrently emitted by the source.

Results and Discussion

Magnetic Properties. The temperature dependence of the magnetic susceptibility of $LaRhSn_2$ is presented in Figure 2. The susceptibilities were only weakly field dependent, indicating only minor amounts of ferromagnetic impurities. The 3 and 5 T data were practically indentical, and we have therefore plotted the 3 T data in Figure 2. Down to about 20 K, the susceptibility is very small and nearly independent of temperature. The small upturn below 20 K is most likely due to a trace amount of paramagnetic impurities, although our Guinier powder patterns showed a single-phase sample. The room-temperature susceptibility is $0.5(2) \times 10^{-9}$ m^3/mol, indicating Pauli paramagnetism, in agreement with the metallic behavior discussed below.

In Figure 3, we present the temperature dependence of the inverse susceptibility of $CeRhSn_2$. Above 50 K we observe Curie−Weiss behavior with a paramagnetic Curie temperature (Weiss constant) of $\theta = -27(2)$ K and an experimental magnetic moment of $\mu_{exp} = 2.56(2)\ \mu_B$/Ce in good agreement with the free ion value for Ce^{3+} of $\mu_{eff} = 2.54\ \mu_B$/Ce. This magnetic behavior is consistent with trivalent cerium. Below 50 K the inverse susceptibility significantly deviates from Curie−Weiss behavior, indicating crystal field splitting of the $J = 5/2$ ground state of the Ce^{3+} ions, but also the beginning of short-range magnetic fluctuations. Crystal field effects may also account for the broad shoulder in the electric resistivity at high temperature (see Figure 6 below). At low temperature (inset of Figure 3) the susceptibility curve shows an anomaly around 4 K indicative for ferro- or ferrimagnetic ordering.

The exact Curie temperature was determined from a kink-point measurement (Figure 4). We have therefore measured the susceptibility in a very low external field of 0.002 T in the zero field cooling and in the field cooling mode. The derivative $d\chi/dT$ of the field cooling measurement resulted in a Curie temperature of $T_c = 4.0(2)$ K.

The magnetization data are plotted in Figure 5. At 20 K, well above the magnetic ordering temperature, the magnetization isotherm is linear as expected for a paramagnetic compound. At 2 K the magnetization did not reach saturation at the highest obtainable field of 5.5 T. The magnetization at 2 K and 5.5 T is only 0.75(2) μ_B/Ce, significantly reduced from the theoretical one for Ce^{3+} of 2.14 μ_B/Ce. Saturation moments in the range of 1 μ_B/Ce atom are frequently observed for similar ternary cerium intermetallics. These small values of the saturation moment are due to crystal field splitting effects on the $J = 5/2$ ground state of the Ce^{3+} ion. The experimentally determined moments per cerium atom are 1.09(5) μ_B for CeAuGe,[5] 1.01(2) μ_B for $CePd_{0.63}Ge_{1.37}$,[10] 0.84 μ_B for $Ce_3Si_2C_2$,[20] and even 0.64 μ_B/Ce for CePtSb.[21] Neutron diffraction experiments are planned to further elucidate the nature of magnetic ordering in $CeRhSn_2$.

Electrical Properties. The temperature dependence of the resistivities of $LaRhSn_2$ and $CeRhSn_2$ is displayed in Figure 6. The resistivity of $LaRhSn_2$ decreases with decreasing temperature as it is typical for a metal. At 4.2 K, the resistivity has dropped to $4 \pm 2\ \mu\Omega$ cm; the room-temperature value is $85 \pm 20\ \mu\Omega$ cm. The large error limit accounts for the different values obtained for several samples. The resistivity ratio $\rho(4.2\text{ K})/\rho(300\text{ K})$ is about 0.04. Features worthy to note in the plot of $CeRhSn_2$ are the broad region of negative curvature roughly centered around 150 K and a broad minimum near 30 K. The latter was also observed for CePdSn[22] and $Ce_3Pd_6Sb_5$[4] and may be due to the presence of some Kondo-like interactions, however, an explanation of increased scattering due to increased magnetic fluctuations as one approaches the ordering temperature is also possible. Since the resistivities could only be measured down to 4.2 K, a further drop at the Curie temperature could not be detected. The resistivities are $100 \pm 20\ \mu\Omega$ cm at 300 K and $45 \pm 10\ \mu\Omega$ cm at 4.2 K, resulting in

(19) Rodriguez-Carvajal, J. FULLPROF Version 2.6.1. Oct. 1994, ILL, unpublished; based on the original code provided by: Wiles D. B.; Sakthivel A. *J. Appl. Crystallogr.* **1981**, *14*, 149.

(20) Gerdes, M. H.; Witte, A. M.; Jeitschko, W.; Lang, A.; Künnen, B. *J. Solid State Chem.* **1998**, *138*, 201.

(21) Rainford, B. D.; Adroja, D. T. *Physica B* **1994**, *194−196*, 365.

(22) Malik, S. K.; Adroja, D. T.; Dhar, S. K.; Vijayaraghavan, R.; Padalia, B. D. *Phys. Rev. B* **1989**, *40*, 2414.

Table 4. Interatomic Distances (pm) in the Structures of $LaRhSn_2$ and $CeRhSn_2$[a]

$LaRhSn_2$										$CeRhSn_2$									
La1:	2	Sn3	321.3(4)	Rh:	2	Sn1	262.6(2)	Sn2:	2	Rh	265.7(4)	Ce1:	2	Sn3	320.1(1)	Rh:	1	Sn2	262.3(1)	Sn2:	2	Rh	262.3(1)
	2	Sn1	326.8(3)		1	Sn2	265.7(4)		1	Sn3	281.2(6)		4	Sn1	323.1(1)		2	Sn1	262.4(1)		1	Sn3	280.9(1)
	4	Sn1	328.7(3)		1	Sn3	268.0(4)		4	Sn1	330.9(3)		2	Sn1	326.8(1)		1	Sn3	266.6(1)		4	Sn1	331.2(1)
	4	Rh	342.3(3)		1	Sn1	277.3(4)		1	La1	351.4(6)		4	Rh	343.9(1)		1	Sn1	277.1(1)		1	Ce1	348.1(2)
	1	Sn2	351.4(6)		2	La2	342.3(3)		4	La2	369.7(2)		1	Sn2	348.1(2)		2	Ce2	339.6(1)		4	Ce2	367.3(1)
	2	Rh	355.5(4)		2	La1	343.9(2)	Sn3:	2	Rh	268.0(4)		2	Rh	352.6(1)		2	Ce1	343.9(1)	Sn3:	2	Rh	266.6(1)
	2	La2	421.7(3)		1	La1	355.5(4)		1	Sn2	281.2(6)		2	Ce2	422.9(1)		1	Ce1	352.6(1)		1	Sn2	280.9(1)
	2	La1	463.9(1)	Sn1:	2	Rh	262.6(2)		2	La1	321.3(4)		2	Ce1	460.3(2)	Sn1:	2	Rh	262.4(1)		2	Ce1	320.1(1)
La2:	4	Rh	343.9(2)		1	Rh	277.3(4)		4	La2	356.6(2)	Ce2:	4	Rh	339.6(1)		1	Rh	277.1(1)		4	Ce2	355.6(1)
	2	Sn1	346.1(3)		1	Sn1	310.4(4)						2	Sn1	347.9(1)		1	Sn1	308.1(1)				
	4	Sn3	356.6(2)		1	La1	326.8(3)						4	Sn3	355.6(1)		2	Ce1	323.1(1)				
	4	Sn2	369.7(2)		2	La1	328.7(3)						4	Sn2	367.2(1)		1	Ce1	326.8(1)				
	2	La1	421.7(3)		2	Sn2	330.9(3)						2	Ce1	422.9(1)		2	Sn2	331.2(1)				
	2	La2	463.9(1)		2	Sn1	342.3(3)						2	Ce2	460.3(2)		2	Sn1	337.9(1)				
	2	La2	481.9(1)		1	La2	346.1(3)						2	Ce2	480.7(2)		1	Ce2	347.9(1)				

[a] All distances of the first coordination spheres are listed. Standard deviations of the least significant digit are given in parentheses.

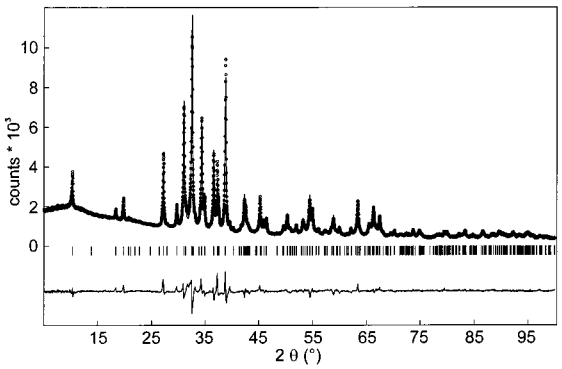

Figure 1. Profile fit and difference plot for the Rietveld refinement of X-ray powder diffraction data for $LaRhSn_2$. The short vertical markers represent allowed reflections.

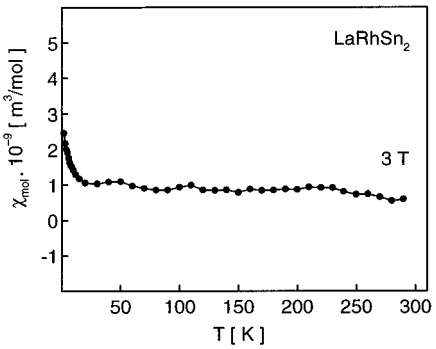

Figure 2. Temperature dependence of the susceptibility of $LaRhSn_2$, measured at a flux density of 3 T.

a resistivity ratio of about 0.45, significantly larger than for $LaRhSn_2$. This is most likely due to magnetic scattering.

^{119}Sn Mössbauer Spectroscopy. Despite the three crystallographically different tin sites in the structures of $LaRhSn_2$ and $CeRhSn_2$, we observe only one signal in the ^{119}Sn Mössbauer spectra (Figure 7). The isomer shifts are $\delta = 1.93(1)$ mm/s ($LaRhSn_2$ 300 K), $\delta = 2.01(2)$ mm/s ($CeRhSn_2$ 78 K), and $\delta = 1.99(2)$ mm/s ($CeRhSn_2$ 4.2 K) with line widths of $\Gamma = 0.86(2)$ mm/s ($LaRhSn_2$ 300 K), $\Gamma = 0.98(2)$ mm/s ($CeRhSn_2$ 78 K), and $\Gamma = 1.01(2)$ mm/s ($CeRhSn_2$ 4.2 K). All spectra are subjected to significant quadrupole splitting of $\Delta E_Q = 1.29(1)$ mm/s ($LaRhSn_2$ 300 K), $\Delta E_Q = 1.38(2)$ mm/s ($CeRhSn_2$ 78 K), and $\Delta E_Q = 1.37(2)$ mm/s ($CeRhSn_2$ 4.2 K). The signals of the three different tin sites are superimposed in the spectra, leading to the slightly

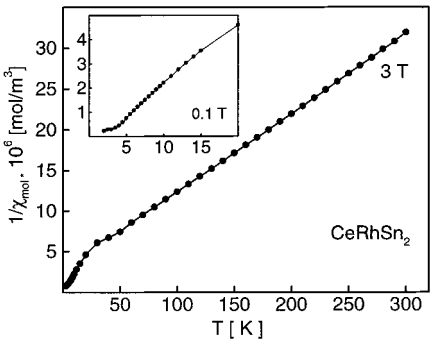

Figure 3. Temperature dependence of the inverse magnetic susceptibility of $CeRhSn_2$ measured at 3 T. The behavior at low temperature and low flux density (0.1 T) is shown in the inset.

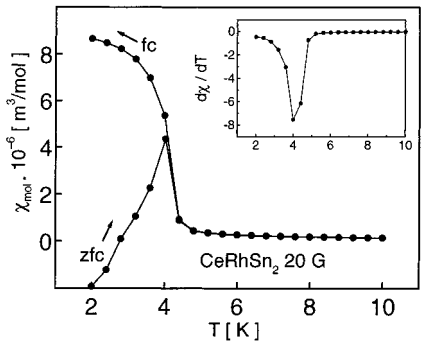

Figure 4. Low-temperature susceptibility (zero field cooling and field cooling modus) of $CeRhSn_2$ at 0.002 T (kink-point measurement). The inset shows the derivative $d\chi/dT$ of the field cooling curve with a sharp peak at the Curie temperature of $T_C = 4.0(2)$ K.

enlarged line widths. A quite similar ^{119}Sn Mössbauer spectrum was observed recently for $CeRu_4Sn_6$.[11] Since the Mössbauer spectrum of $CeRhSn_2$ was measured at 4.2 K (slightly above the magnetic ordering temperature of 4.0 K), no magnetic hyperfine field splitting due to a transferred field is detected at the tin nucleus.

Crystal Chemistry and Chemical Bonding. The ternary stannides $LaRhSn_2$ and $CeRhSn_2$ crystallize with a new orthorhombic structure type which we have first determined for the cerium compound. We therefore call this a $CeRhSn_2$-type structure. In the following discussion, when we quote interatomic distances we refer to the distances in $CeRhSn_2$, since they are more accurate than those for $LaRhSn_2$.

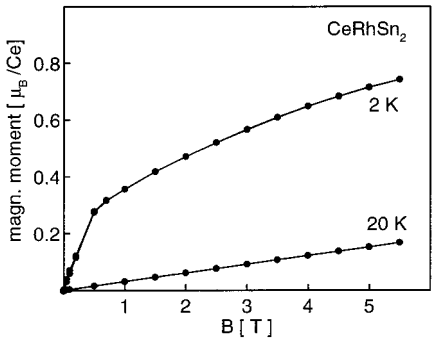

Figure 5. Field dependence of the magnetic moment of $CeRhSn_2$ at 2 and 20 K.

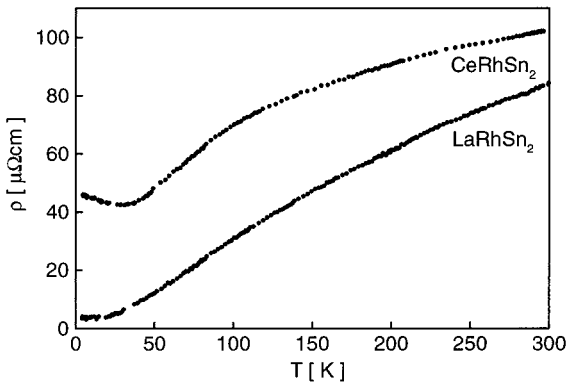

Figure 6. Temperature dependence of the resistivities of $LaRhSn_2$ and $CeRhSn_2$.

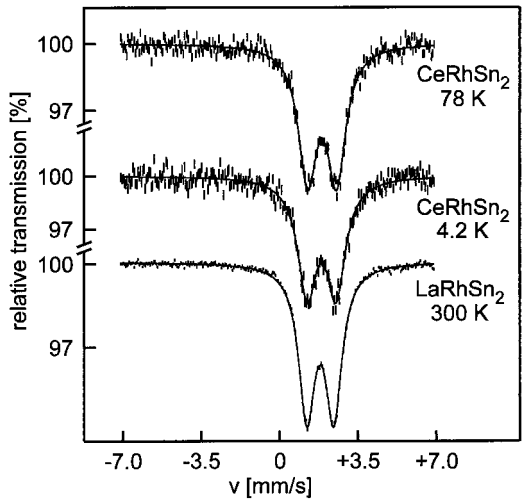

Figure 7. Experimental and simulated ^{119}Sn Mössbauer spectra of $LaRhSn_2$ (300 K) and $CeRhSn_2$ (78 and 4.2 K) relative to $Ca^{119}SnO_3$.

The two crystallographically independent cerium atoms (Figure 8) have high coordination numbers (CN): 4Ce + 6Rh + 9Sn for Ce1 and 6Ce + 4Rh + 10Sn for Ce2, resulting in CN19 and CN20, respectively. These high coordination numbers are typical for such intermetallic compounds. The Ce−Rh distances range from 340 to 353 pm, significantly longer than the sum of the metallic radii[23] of 317 pm for CN12, indicating only negligible Ce−Rh interactions. The Ce−Sn distances cover the wide range from 320 to 367 pm with an average value of 343 pm, in good agreement with

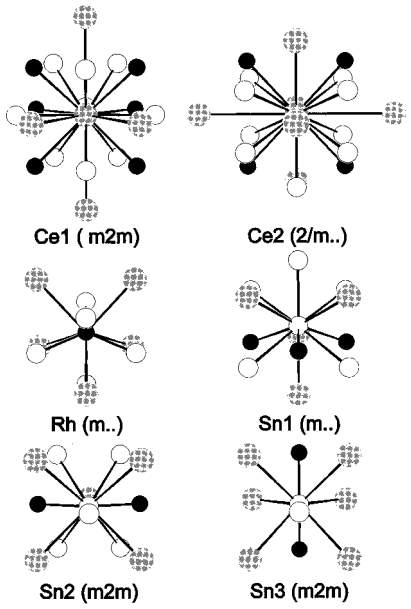

Figure 8. Near-neighbor environment in $CeRhSn_2$. The site symmetries are given in parentheses.

the sum of the metallic radii[23] for cerium and tin of 345 pm. It is worthwhile to note, however, that the eight nearest tin neighbors of Ce1 have Ce−Sn distances from 320 to 327 pm. These contacts are most likely bonding. A comparable situation is observed for $CeRu_4Sn_6$,[11] where each cerium atom has 12 tin neighbors at Ce−Sn distances ranging from 336 to 371 pm.

The Ce−Ce distances range from 423 to 481 pm, much longer than in *fcc* cerium[24] where each cerium atom has 12 cerium neighbors at 365 pm. In $CeRhSn_2$ the Ce−Ce distances are well above the Hill limit[25] of about 340 pm for f electron localization, in agreement with magnetic ordering discussed above.

The most striking feature of the $CeRhSn_2$ structure are the short Rh−Sn distances. Each rhodium atom has five tin neighbors at Rh−Sn distances ranging from 262 to 277 pm in the form of an elongated, distorted square pyramid. These Rh−Sn distances compare well with the sum of Paulings single bond radii[26] of 265 pm for rhodium and tin. We therefore assume strong rhodium−tin bonding in the structure of $CeRhSn_2$.

The three crystallographically different tin atoms (Figure 8) have different coordination spheres. Sn1 and Sn2 both have CN12: 3Rh + 4Ce + 5Sn for Sn1 and 2Rh + 5Ce + 5Sn for Sn2. The Sn3 atoms have the lower CN9 with 2Rh + 6Ce + 1Sn. The most striking difference in the coordination of the tin atoms is the variation of the Sn−Sn distances. The Sn3 atoms have only one Sn2 neighbor at 281 pm. This is exactly the Sn−Sn single bond distance in the diamond modification of tin (α-Sn).[24] The second remarkable distance is the Sn1−Sn1 bond length of 308 pm. In view of the Sn−Sn distances in β-tin[24] (4 × 302 pm; 2 × 318 pm), the Sn1−Sn1 contacts are also most likely bonding. The Sn−Sn

(23) Teatum, E.; Gschneidner, K., Jr.; Waber, J. Rep. LA-2345, U.S. Department of Commerce: Washington, DC, 1960.

(24) Donohue, J. *The Structures of the Elements*; Wiley: New York, 1974.

(25) Hill, H. H. In *Plutonium and other Actinides*; Mines, W. N., Ed.; Nuclear Materials Series, AIME: New York, 1970; Vol. 17, p 2.

(26) Pauling, L. *The Nature of the Chemical Bond and the Structures of Molecules and Solids*; Cornell University Press: Ithaca, NY, 1960.

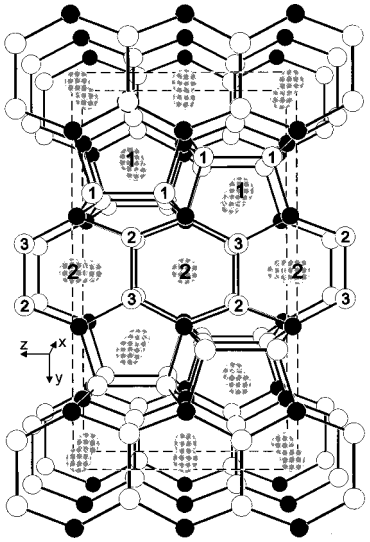

Figure 9. View of the crystal structure of $CeRhSn_2$ approximately along the *x* axis. The cerium, rhodium, and tin atoms are drawn as gray, black, and open circles, respectively. The three-dimensional $[RhSn_2]$ polyanion is emphasized. Only Rh−Sn and the shortest Sn−Sn distances are drawn.

distances between the Sn1−Sn1 and Sn2−Sn3 dumbbells of 331 and 338 pm are much longer. These contacts are only weakly bonding.

In a first approximation, one might consider both tin dumbbells as $(Sn1-Sn1)^{6-}$ and $(Sn2-Sn3)^{6-}$, assuming single bond character. The cerium atoms as the most ignoble component of our compound have transferred their three valence electrons to the tin atoms. The formula of $CeRhSn_2$ can then be written as $[2Ce^{3+}]^{6+}$-$[2Rh^{3+}]^{6+}[Sn1-Sn1]^{6-}[Sn2-Sn3],^{6-}$ where the superscripts are formal charges. In this formulation the rhodium atoms have a d^6 configuration. In a simple MO scheme a d^6 low-spin configuration is possible for a distorted square pyramid[27] and consequently the rhodium atoms give no magnetic contribution as shown by the Pauli paramagnetism of $LaRhSn_2$.

As mentioned above, the remarkable structural motif of the $CeRhSn_2$ structure is the distorted $RhSn_5$ square pyramid. These pyramids are condensed with each other via common tin atoms and via Sn−Sn bonds (Sn1−Sn1 and Sn2−Sn3), thus forming a three-dimensional polyanion. In emphasizing the essentially covalent bonding within this polyanion we can write $Ce^{3+}[RhSn_2]^{3-}$. The cerium atoms are located within distorted pentagonal and hexagonal channels of the polyanion (Figure 9).

Finally it is worthwhile to note that two closely related phases exist. In the ternary system lanthanum−rhodium−tin the stannides $LaRh_{0.36(2)}Sn_2$ and $LaRh_{0.69(2)}Sn_2$ with defect $CeNiSi_2$-type structure have been reported.[28] With the ideal composition, the $CeRhSn_2$ type, described in the present paper, occurs. This compound has a composition (in atomic percentage) of 25:25:50. Interestingly, also $Ce_5Rh_4Sn_{10}$ (26.3:21.1:52.6)[29] with a very similar composition exists. However, both stannides have distinctly different crystal structures.

Acknowledgment. We are indebted to Professor Wolfgang Jeitschko and to Professor Hellmut Eckert for their interest and steady support of this work. We also thank Klaus Wagner for the EDX analyses, Dr. Rolf-Dieter Hoffmann for the collection of the X-ray powder data, and Dr. Wolfgang Gerhartz (Degussa AG) for a generous gift of rhodium powder. Financial support by the Benningsen-Foeder-Programm of the Ministerium für Wissenschaft und Forschung des Landes Nordrhein-Westfalen, by the Deutsche Forschungsgemeinschaft and by the Fonds der Chemischen Industrie is gratefully acknowledged.

CM991006U

(27) Holleman-Wiberg. *Lehrbuch der Anorganischen Chemie*, 101th ed.; Wiberg, N., Ed.; de Gruyter; Berlin, 1995.
(28) François, M.; Venturini, G.; Malaman, B.; Roques, B. *J. Less-Common Met.* **1990**, *160*, 197.
(29) Venturini, G.; Malaman, B.; Roques, B. *Mater. Res. Bull.* **1989**, *24*, 1135.